On the origin of the open-circuit voltage of polymer–fullerene solar cells

Koen Vandewal[1]*, Kristofer Tvingstedt[2], Abay Gadisa[1], Olle Inganäs[2] and Jean V. Manca[1]

The increasing amount of research on solution-processable, organic donor–acceptor bulk heterojunction photovoltaic systems, based on blends of conjugated polymers and fullerenes has resulted in devices with an overall power-conversion efficiency of 6%. For the best devices, absorbed photon-to-electron quantum efficiencies approaching 100% have been shown. Besides the produced current, the overall efficiency depends critically on the generated photovoltage. Therefore, understanding and optimization of the open-circuit voltage (V_{oc}) of organic solar cells is of high importance. Here, we demonstrate that charge-transfer absorption and emission are shown to be related to each other and V_{oc} in accordance with the assumptions of the detailed balance and quasi-equilibrium theory. We underline the importance of the weak ground-state interaction between the polymer and the fullerene and we confirm that V_{oc} is determined by the formation of these states. Our work further suggests alternative pathways to improve V_{oc} of donor–acceptor devices.

The most successful solution-processable organic solar cells use a C_{60} or C_{70} fullerene derivative as an electron acceptor blended with a conjugated polymer[1–3]. In the field, attempts have been made to derive upper limits for the efficiency of this type of polymer–fullerene photovoltaic device, albeit with empirical arguments related to the details of the origin of the open-circuit voltage[3–5] (V_{oc}). However, as energy is converted from one form (radiation) to another (electrical), fundamental losses should be taken into account and it should be possible to derive an upper limit for V_{oc}, purely on the basis of thermodynamic considerations. For single absorber materials, this fundamental question was answered in 1961 in a seminal paper by Shockley and Queisser[6]. Their analysis was based on the detailed balance of absorption and emission events from the solar cell, a 'grey' body at the surface of the Earth, illuminated by the Sun, a black body of much higher temperature. This allowed the derivation of an expression for V_{oc} as a function of the material's bandgap. It was found that V_{oc} is maximal for the ideal case in which the charges can recombine only radiatively.

According to this reasoning, it is clear that the V_{oc} of polymer–fullerene devices has not reached its thermodynamic maximal value yet. This value would be reached if the only recombination mechanism at open-circuit conditions is a radiative one[6]. As a result of the severe luminescence quenching in material blends yielding a substantial charge generation, it is clear that radiative recombination is just a small fraction of the total recombination, and a reduction of the maximum obtainable V_{oc} is expected. In fact, no correlations of V_{oc} with the optical gap of any of the blend constituents, as predicted by Shockley and Queisser[6], are observed. Instead, V_{oc} is found to scale with the difference between the highest occupied molecular orbital energy of the donor and the lowest unoccupied molecular orbital energy of the fullerene acceptor[4,7]. This leads to the conclusion that in this type of solar cell, the V_{oc} is determined by recombination at the donor/acceptor interface[8–12].

Recently, for some polymer–fullerene blends, radiative interface recombination was observed. The presence of a weak emission signal, redshifted compared to the pure components, was detected in the photoluminescence and electroluminescence spectra and

was assigned to the emission of interface electron–hole pairs or charge-transfer excitons[13–17]. The signature of this emitting state is also present in the absorption spectrum as a new, weak subgap absorption band in several polymer–fullerene blends used for photovoltaic applications[18–20]. Such absorption bands are typical for the formation of a ground-state charge-transfer complex (CTC) between the polymer and the fullerene. Furthermore, good correlations between the open-circuit voltage and the spectral position of the charge-transfer absorption[20], photoluminescence[15] or electroluminescence[17] could be made.

Here, we show that the electroluminescence and photovoltaic external quantum efficiency spectra in the low-energy, charge-transfer region are related to each other as predicted by the detailed balance approach. Furthermore, it is shown that at V_{oc}, the photocurrent generated by the absorption of sunlight balances with the recombination current, resulting in emission of photons by the excited CTCs. This confirms previous suggestions[10,15,20], that V_{oc} is determined by the CTC formation between the polymer and the fullerene.

To validate the generality of the detailed balance treatment for polymer–fullerene solar cells, blends of five different donor polymers and two fullerene derivatives, that is, [6,6]-phenyl C61 butyric acid methyl ester ($PC_{61}BM$) and [6,6]-phenyl C71 butyric acid methyl ester ($PC_{71}BM$), were investigated. The polymers belong to different conjugated polymer material families, comprising different conjugated backbones. These conjugated polymers are representative of the donor polymers used in polymer–fullerene solar cells explored in the community at present. Their chemical structures are shown in Fig. 1.

Devices based on poly[2-methoxy-5-(30,70-dimethyloctyloxy)-1,4-phenylene vinylene] (MDMO-PPV) and poly[2,7-(9-di-octyl-fluorene)-alt-5,5-(4′,7′-di-2-thienyl-2′,1′,3′ benzothiadiazole)] (APFO3) were prepared using different polymer/fullerene stoichiometries. Optimal devices were obtained using a 1:4 polymer/fullerene weight ratio, resulting in a power conversion efficiency of ~2% and ~2.5% respectively. At a lower fullerene content, the photogenerated current becomes lower and the

[1]IMEC-IMOMEC, vzw, Institute for Materials Research, Hasselt University, Wetenschapspark 1, 3590 Diepenbeek, Belgium, [2]Biomolecular and Organic Electronics, Center of Organic Electronics (COE), Department of Physics, Chemistry and Biology, Linköping University, 58183 Linköping, Sweden.
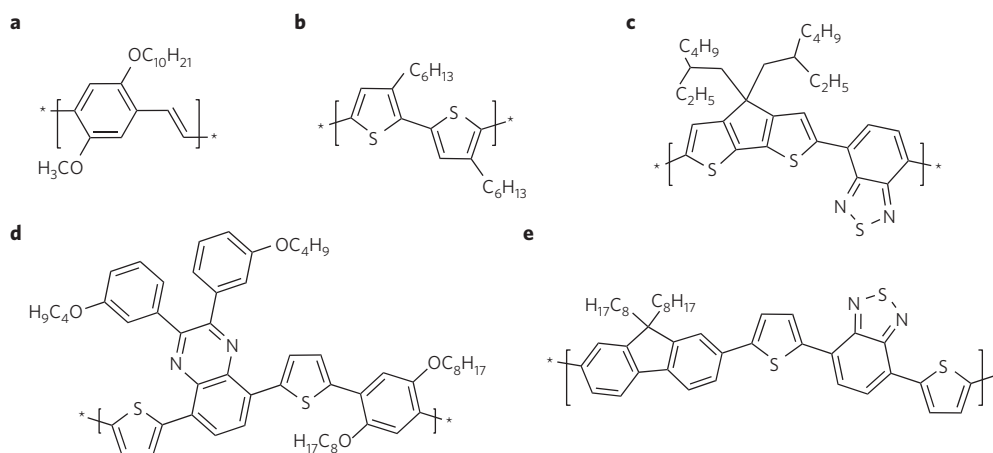*e-mail: koen.vandewal@uhasselt.be.

Figure 1 | The chemical structures of the donor polymers used. a, MDMO-PPV. **b**, P3HT. **c**, PCPDTBT. **d**, LBPP5. **e**, APFO3.

Table 1 | Measured J_{sc}, V_{oc} and calculated J_0 for all of the devices studied in this work.

Material	J_{sc} (A m^2)	V_{oc} (V)	J_0 (A m^{-2})
P3HT–PC$_{61}$BM (1:1)			
annealed	81 (±8)	0.62 (±0.01)	1.3 (±0.9) E-9
as prepared	35 (±8)	0.76 (±0.03)	5.6 (±3.0) E-12
PCPDTBT–PC$_{61}$BM (1:2)			
with octyldithiols	100 (±5)	0.64 (±0.01)	1.9 (±1.1) E-9
without octyldithiols	66 (±7)	0.67 (±0.01)	6.7 (±5.3) E-11
LBPP5–PC$_{71}$BM (1:3)			
	45 (±9)	0.73 (±0.015)	5.4 (±2.1) E-12
MDMO-PPV–PC$_{61}$BM			
1:4	34 (±7)	0.83 (±0.02)	2.2 (±0.8) E-13
1:1	14 (±2)	0.88 (±0.01)	1.1 (±0.4) E-14
4:1	3 (±0.6)	0.92 (±0.02)	3.8 (±2.2) E-15
APFO3–PC$_{61}$BM			
1:4	45 (±5)	1.02 (±0.01)	1.6 (±0.6) E-16
1:1	28 (±4)	1.08 (±0.015)	2.7 (±1.0) E-18
4:1	10 (±1)	1.16 (±0.01)	1.3 (±0.8) E-19
APFO3–PC$_{71}$BM			
1:4	35 (±5)	0.98 (±0.01)	1.5 (±0.3) E-16
1:1	30 (±3)	1.00 (±0.01)	1.0 (±0.2) E-16
4:1	10 (±2)	1.13 (±0.01)	6.6 (±4.4) E-19

J_0 was calculated using the $EQE_{PV}(E)$ and $EQE_{EL}(E)$ spectra by means of equation (3). The errors on J_{sc} and V_{oc} are experimental errors obtained by measuring different devices. For the errors on J_0, the variation of J_0 over the spectral range of the CTC was taken into account as well as the experimental error on EQE_{EL}.

Figure 2 | The EQE_{PV} spectra of polymer–fullerene devices. The devices comprise active layers: P3HT–PC$_{61}$BM (1:1) (annealed), PCPDTBT–PC$_{61}$BM (1:2), LBPP5–PC$_{71}$BM (1:3), MDMO-PPV–PC$_{61}$BM (1:4) and APFO3–PC$_{61}$BM (1:4). **a**, The spectra on a linear scale. The standard AM1.5 G spectrum is shown on the right axis. **b**, The spectra on a logarithmic scale, to make the weak contribution of the low oscillator strength CTC visible. A charge-transfer band is clearly visible for all five material blends. Depending on the donor polymer, the spectral position of the charge-transfer band varies. On the right axis of **b**, the emission spectrum of a black body at room temperature is shown.

efficiency drops. However, V_{oc} increases as the fullerene content is decreased (see Supplementary Information). APFO3-based devices were prepared with both PC$_{61}$BM and PC$_{71}$BM. For the poly[3-hexylthiophene] (P3HT)–PC$_{61}$BM blends, ordering of the polymer phase, for example, induced by annealing, has been proven to have a major influence on the device performance[21]. Therefore, in this study, as-prepared and annealed devices were characterized. For this material system, typical conversion efficiencies of 3.5% were reached. However, higher efficiencies for P3HT–PC$_{61}$BM devices of up to 5% have been reported[22]. A polymer of particular interest is poly[2,6-(4,4-bis-(2-ethylhexyl)-4H-cyclopenta[2,1-b;3,4-b′]-dithiophene)-alt-4,7-(2,1,3-benzothiadiazole)] (PCPDTBT), as it has a low optical gap, close to the optimum as predicted by Shockley and Queisser[6]. It was shown that the addition of thiols in a PCPDTBT–fullerene solution improves the device performance[23]. We obtained for PCPDTBT–PC$_{61}$BM devices typically a power conversion efficiency of 3%. Efficiencies of 5.5% were reported for
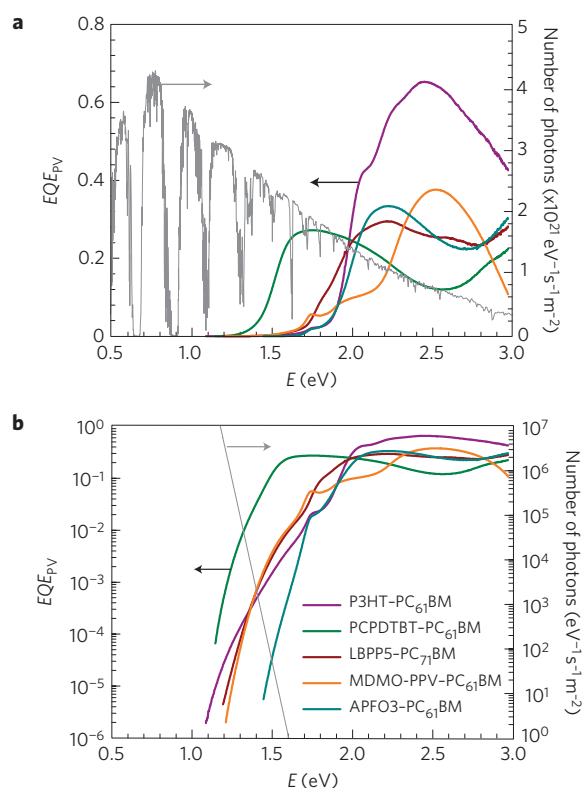
PCPDTBT–PC$_{71}$BM devices[23]. As in this article, there is particular interest in the V_{oc} of the devices; note that the obtained V_{oc} values correspond to what is found in the literature for similar devices. An overview of the devices studied in this work and the measured short-circuit current (J_{sc}) and V_{oc} values are listed in Table 1.

In Fig. 2a, photovoltaic external quantum efficiency (EQE_{PV}) spectra are shown on a linear scale for five devices using the
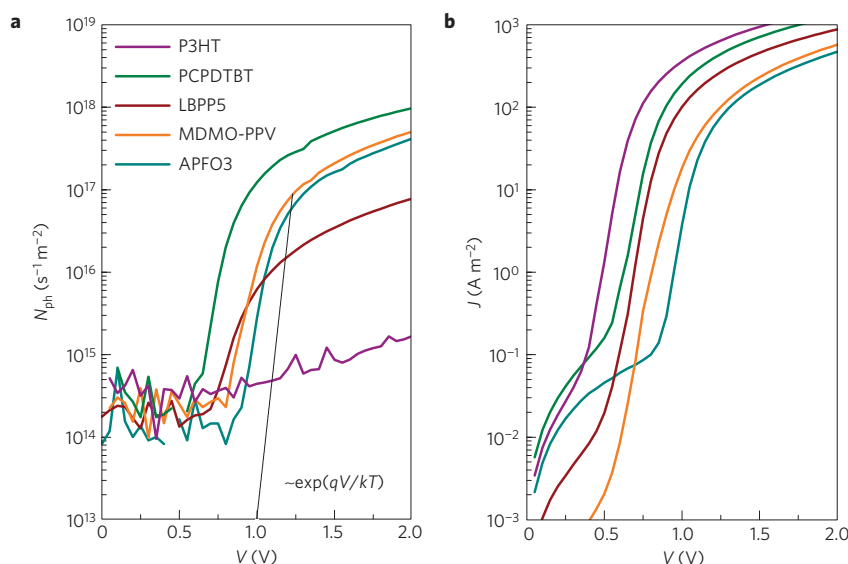
Figure 3 | Electroluminescence emission and corresponding injected current versus voltage curves of polymer–fullerene devices. The active layers of the devices are: P3HT–PC$_{61}$BM (1:1) (annealed), PCPDTBT–PC$_{61}$BM (1:2), LBPP5–PC$_{71}$BM (1:3), MDMO-PPV–PC$_{61}$BM (1:4) and APFO3–PC$_{61}$BM (1:4). **a**, The number of detected photons by a silicon detector versus the applied voltage over the device. The black line represents a curve proportional to exp(qV/kT). An onset proportional to this curve is measurable for all polymer–fullerene devices, except for the annealed P3HT–PC$_{61}$BM device, because of its low-efficiency electroluminescence. **b**, The corresponding injection current versus voltage curves.

above conjugated polymers. Spectra for further devices using different preparation conditions are shown in the Supplementary Information. For the P3HT-, MDMO-PPV-, APFO3- and poly[1,4-(2,5-dioctyloxybenzene)-alt-5,5-(5′,8′-di-2-thienyl-2′,3′-di-(3″-butoxyphenyl)quinoxaline)] (LBPP5)-based devices, the fullerene has the lowest optical gap of the blend constituents (1.7 eV). For the PCPDTBT–PC$_{61}$BM device however, the lowest optical gap is the polymer bandgap (1.4 eV). From these EQE_{PV} spectra, the total photogenerated current can be calculated, by integrating the EQE_{PV} spectrum over the solar spectrum, shown on the right axis of Fig. 2a. From this figure, it is clear that the photocurrent under solar illumination for these five devices is dominated by polymer absorption. In this respect, the use of a C$_{70}$ fullerene derivative is beneficial, as it aids in absorbing a substantially greater part of the sunlight than the C$_{60}$ derivative[24].

Polymer–fullerene ground-state material interaction and CTC formation is characterized by the presence of a new absorption band, owing to an optical transition in which an electronic charge is transferred from the donor-conjugated polymer to the fullerene acceptor. The low oscillator strength of this transition and hence low absorption coefficient however, forces us to use specialized techniques to detect charge-transfer bands in the $EQE_{PV}(E)$ spectra. Therefore, the sensitive detection method Fourier-transform photocurrent spectroscopy[20,25] (FTPS) is also used to collect the very low photocurrent signals generated by excitation of the CTCs. These signals become visible in the $EQE_{PV}(E)$ spectra, shown in Fig. 2b on a logarithmic scale. For all five material combinations shown in the figure and the combinations shown in the Supplementary Information, the lowest energy excitation is due to a charge-transfer optical transition. Depending on the donor polymer, this subgap charge-transfer band has an onset ranging from 1 to 1.5 eV.

In Fig. 3, the total number of photons N_{ph} emitted by electroluminescence and detected by a silicon detector, versus voltage, and the corresponding injected current $J_{inj}(V)$ for the five material combinations are shown. It can be seen that the electroluminescence emission onset is proportional to exp(qV/kT). Here, k is the Boltzmann constant, T is the absolute room temperature and q is the elementary electron charge. This onset

is lower than the voltage onset of the electroluminescence of the pure materials[17]. At high voltages, the electroluminescence and injected current are space-charge and/or series-resistance limited and deviate from the exponential. Owing to the low quantum efficiency of the charge-transfer emission of annealed P3HT–PC$_{61}$BM devices and the limited detection range of the Si photodiode, the exponential part in the electroluminescence versus voltage curves could not be resolved for this device.

To spectrally resolve the electroluminescence spectra with a sufficiently high signal, they were measured with a sensitive set-up using injection currents corresponding to a charge density present in the device comparable to 1–10 sun conditions. As the total number of photons emitted by electroluminescence scales with the injected current, we choose to show the electroluminescence external quantum efficiency (EQE_{EL}), calculated as the number of emitted photons divided by the number of injected electrons. These spectra are shown in Fig. 4a. In contrast to the $EQE_{PV}(E)$ spectra in Fig. 2, the $EQE_{EL}(E)$ spectra are dominated by charge-transfer emission, and substantially redshifted as compared with the emission of the pure components[15–17]. The overall, integrated EQE_{EL} for all samples is very low, ranging from 10^{-9} to 10^{-6}.

We will now use the principle of detailed balance to make a connection between the low-energy, charge-transfer-dominated part of the $EQE_{PV}(E)$ and $EQE_{EL}(E)$ spectra, and to relate these spectra to V_{oc}. In this respect, Würfel derived a generalized Planck law for systems in quasi-equilibrium, including a chemical potential of radiation equal to the splitting of the quasi-Fermi levels[26]. It was shown to be valid for inorganic solar cells[27] and dye-sensitized solar cells[28]. Similar approaches were used to relate photoluminescence spectra to the absorption spectra of organic materials[29] and to calculate the free energy available in photosynthetic systems[30]. Extensions were made for third-generation photovoltaics[31]. A useful equation, similar to Würfel's generalized Planck law, was recently introduced by Rau, relating the photovoltaic and electroluminescent actions of solar cells[32].

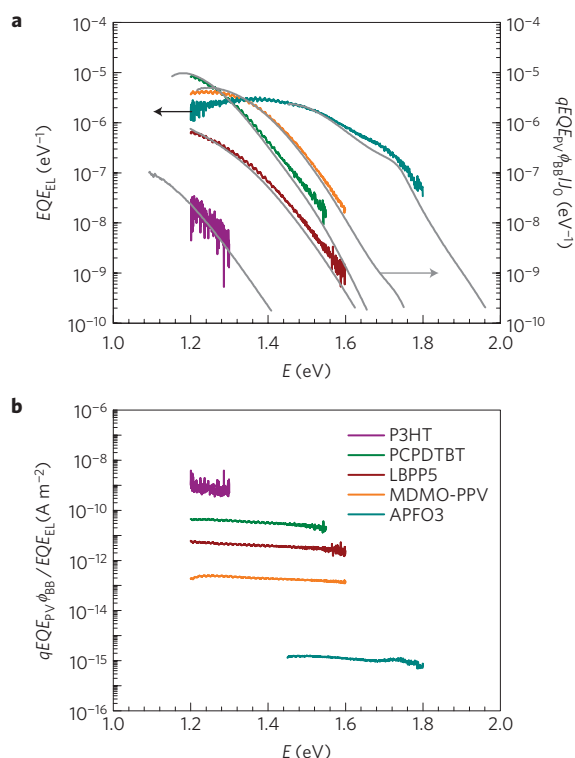$$\phi_{EL}(E,V) = EQE_{PV}(E)\phi_{BB}(E)\left(\exp\left(\frac{qV}{kT}\right)-1\right) \quad (1)$$

Figure 4 | Comparison of the measured EQE_{EL} with the product of the EQE_{PV} spectrum with the black-body spectrum at room temperature. a, Left axis: The EQE_{EL} spectra devices based on the material blends P3HT–PC$_{61}$BM (1:1) (annealed), PCPDTBT–PC$_{61}$BM (1:2), LBPP5–PC$_{71}$BM (1:3), MDMO-PPV–PC$_{61}$BM (1:4) and APFO3–PC$_{61}$BM (1:4). These EQE_{EL} were obtained using injection currents in the range (1–10) times J_{sc}. Right axis: EQE_{EL} spectra, proportional to the product of the EQE_{PV} spectrum with the black-body spectrum at room temperature. **b,** The ratio of the EQE_{PV} and EQE_{EL} multiplied by the black-body spectrum at room temperature. This value is fairly constant over the low-energy spectral region and equals J_0.

Here, $\phi_{EL}(E, V)$ is the excess electroluminescence spectral photon flux and $\phi_{BB}(E)$ is the black-body spectrum at 300 K, integrated over all possible incidence angles. The $\phi_{BB}(E)$ spectrum is shown on the right axis of Fig. 2b. Note that this is an exponentially decreasing function with increasing photon energy, making only the low-energy part of $EQE_{PV}(E)$ important in the evaluation of equation (1). For a low-mobility organic metal–insulator–metal, it was recently shown that relation (1) becomes only approximately valid[33]. However, the deviations are expected to be within one order of magnitude.

A simple relationship between $EQE_{EL}(E)$ and $EQE_{PV}(E)$ can be deduced if the ideal diode equation is used to describe the injected current $J_{inj}(V)$:

$$J_{inj}(V) = J_0\left(\exp\left(\frac{qV}{kT}\right) - 1\right) \quad (2)$$

Here, J_0 is the dark saturation current. We can deduce the following relationship between the EQE_{PV} and EQE_{EL} spectra:

$$J_0 EQE_{EL}(E) = q EQE_{PV}(E)\phi_{BB}(E) \quad (3)$$

Here, J_0 is assumed to be implicitly voltage dependent, to maintain the generality of equation (2) for the description of dark $I–V$ curves of polymer–fullerene devices. Typically, J_0 is determined
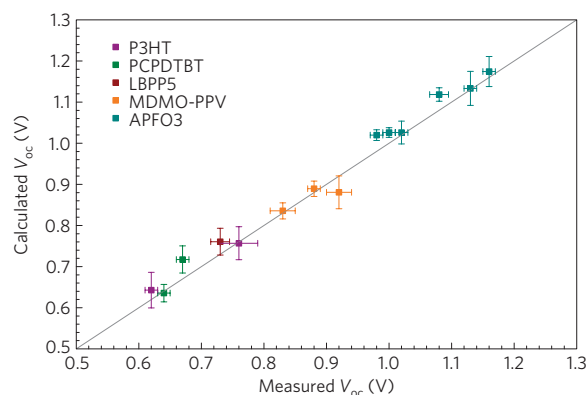

Figure 5 | The V_{oc} obtained by means of the detailed balance approach versus the measured V_{oc}. The different colours indicate devices based on different donor polymers: P3HT–PC$_{61}$BM (1:1), PCPDTBT–PC$_{61}$BM (1:2), LBPP5–PC$_{71}$BM (1:3), MDMO-PPV–PC$_{61}$BM, APFO3–PC$_{61}$BM and APFO3–PC$_{71}$BM. Measured and calculated V_{oc} values were obtained for freshly prepared and annealed P3HT-based devices. For MDMO-PPV–PC$_{61}$BM, APFO3–PC$_{61}$BM and APFO3–PC$_{71}$BM, the stochiometry was changed (4:1, 1:1, 1:4). PCPDTBT–PC$_{61}$BM (1:2) was studied with and without the addition of octyldithiols in the solution. The grey line is a one-to-one correspondence. Experimental errors on the measured V_{oc} were obtained by measuring different samples. Error bars on the V_{oc} calculated by means of detailed balance were obtained by using the errors on the calculated J_0 and the absolute value of the measured EQE_{EL}.

by injection and recombination mechanisms of the free carriers[34]. For polymer–fullerene blends, diode equations with ideality factors between one and two are often used[35]. In the notation used here, J_0 is in that case exponentially dependent on voltage. See the Supplementary Information for further details regarding J_0 and the ideality factor.

Equation (3) relates the shape of the $EQE_{PV}(E)$ spectrum to the shape of the $EQE_{EL}(E)$ spectrum. The validity of this simple relation for polymer–fullerene solar cells is shown in Fig. 3a. It can be seen that multiplying $EQE_{PV}(E)$ by the ambient black-body spectrum $\phi_{BB}(E)$, the charge-transfer-dominated $EQE_{EL}(E)$ of all photovoltaic devices comprising our five different donor polymers is obtained within acceptable limits. Note that these relations are valid also for large Stokes shifts between the charge-transfer absorption and emission.

Furthermore, using equation (3), a value for J_0 can be deduced, by taking the ratio between $q EQE_{PV}(E)\phi_{BB}(E)$ and $EQE_{EL}(E)$. Here, EQE_{EL} is measured under injection conditions equivalent to 1–10 suns, whereas $EQE_{PV}(E)$ was measured under short-circuit conditions. Note that J_0 obtained in this way is fairly constant over the range of overlapping $EQE_{PV}(E)$ and $EQE_{EL}(E)$. Only a slight decrease of J_0 with increasing photon energy is observed. This is at least partly due to the fact that during the EQE_{EL} measurements, current is injected into the device, causing the effective temperature of the devices to increase as compared with room temperature. This heating slightly broadens the emission bands and causes the observed small slope. Further experimental errors on J_0 originate from the experimental errors on the absolute EQE_{EL}. The obtained J_0 values for all investigated photovoltaic devices with their experimental errors are listed in Table 1.

Integrating equation (3) yields the following expression for J_0:

$$J_0 = \frac{q}{EQE_{EL}} \int EQE_{PV}(E)\phi_{BB}(E)\,dE \quad (4)$$

Here, EQE_{EL} is the overall electroluminescence external quantum efficiency, obtained by integrating $EQE_{EL}(E)$ over all photon

energies. The essential contribution of $EQE_{PV}(E)$ to the integral in equation (4) is in fact only the low-energy charge-transfer part, as ϕ_{BB} is exponentially decreasing with increasing photon energy. This is in correspondence with the suggestion made by Potscavage et al.[10] that the dark current originates from thermal excitations of ground-state charge-transfer complexes.

At open circuit, the injected current $J_{inj}(V)$ causing the low-quantum-efficiency charge-transfer emission equals J_{sc}; hence, by reforming equation (2), we obtain a commonly used equation for V_{oc}:

$$V_{oc} = \frac{kT}{q} \ln\left(\frac{J_{sc}}{J_0} + 1\right) \qquad (5)$$

Note that this formula for V_{oc} does not contain a parameter related explicitly to any optical gap. Spectral band positions are present in the equation implicitly in the term J_0 through equation (3). Note that, as both J_0 and J_{sc} are proportional to respectively $\phi_{BB}(E)$ and the AM1.5 spectrum integrated over $EQE_{PV}(E)$, their ratio is determined by the spectral shape of $EQE_{PV}(E)$ alone, which was measured at short circuit in this work. Furthermore, this formula is expected to be valid if the injected current is diode-like, as it is for the devices investigated in this work at voltages comparable to V_{oc} (Fig. 3).

To check the validity of equation (5), J_0 is obtained as described above. J_{sc} is obtained by integrating the EQE_{PV} spectrum over the solar spectrum or by measuring it directly under solar illumination. Experimental errors on J_{sc} were obtained by comparing the calculated data with the measured data of several devices on different solar simulators. The used J_{sc} values with their experimental errors of all the devices studied in this work are listed in Table 1.

The V_{oc} values calculated by means of detailed balance versus the measured V_{oc} values are shown in Fig. 5 for all studied devices comprising the five investigated polymers, using different preparation conditions. An overview of all preparation conditions is shown in the Supplementary Information. Excellent correspondence of the measured V_{oc} with the calculated V_{oc} is observed and differences in V_{oc} on changing preparation conditions, such as stoichiometry alterations and annealing, are accurately reproduced. These differences in V_{oc} are interpreted as being mainly caused by the spectral shifts of the charge-transfer bands on changing the preparation conditions[13,18].

The obtained new insights reveal pathways to increase the V_{oc} of polymer–fullerene devices. From equation (4) it is clear that, because of the exponential nature of $\phi_{BB}(E)$ a blueshift of the charge-transfer band results in an exponential decrease of J_0 through the term $EQE_{PV}(E)\phi_{BB}(E)$. Owing to the logarithmic dependence of V_{oc} on J_0 (equation (5)), V_{oc} depends linearly on the spectral position of the charge-transfer band. This results in the good correlations of V_{oc} with the onset of the charge-transfer band[20] or the peak of charge-transfer emission[15,17].

The spectral position of the charge-transfer band is mainly determined by the energetic difference between the highest occupied molecular orbital of the donor polymer to the lowest unoccupied molecular orbital of the electron acceptor[36–38]. The presented theoretical approach explains the widely observed correlation between V_{oc} and this energy level difference. However, there are other factors influencing the spectral position of the charge-transfer band, such as the binding energy of the charge-transfer exciton and its electrostatic environment[36–38].

Up to now, increasing the lowest unoccupied molecular orbital level of the fullerene[39,40] or using donor polymers with optimized energetic levels[41], have been the most followed pathways for increasing the V_{oc} of polymer–fullerene solar cells. From equation (5) however, other pathways for increasing V_{oc} become apparent. Reducing the electronic coupling between the polymer

and the fullerene will suppress the charge-transfer band oscillator strength and will reduce J_0, and thus increase V_{oc}. The fact that V_{oc} can also depend on the coupling between donor and acceptor material, was recently shown by Perez and colleagues[42].

In the devices studied here, the recombination rate exceeds many times the charge-transfer emission rate, hence the low EQE_{EL} in the studied devices. At solar illumination conditions, values of EQE_{EL} are of the order of 10^{-6} or 10^{-9}. Increasing EQE_{EL}, by eliminating the extra non-radiative pathways and thus improving the carrier lifetime, will result in a decrease of J_0 (formula (5)) and therefore an increase in V_{oc}.

The theoretical maximum V_{oc} will be obtained at EQE_{EL} equals unity. This means that all non-radiative pathways are eliminated, resulting in a maximum charge-carrier lifetime, only determined by radiative recombination. Note that even in this case V_{oc} does not necessarily equal the optical gap of the material blend, as fundamental thermodynamic losses owing to entropy creation will always cause the potential of the device to be lower than the energy of the relaxed charge-transfer exciton. From equations (4) and (5), we can deduce that, increasing EQE_{EL} by a factor of 10 will result in an increase in V_{oc} of ~58 mV at room-temperature conditions. This means that for polymer–fullerene solar cells, for which $EQE_{EL} \sim 10^{-9}–10^{-6}$, 0.5–0.3 V is still to be gained, by eliminating the non-radiative recombination pathways, if this is possible. Therefore, to improve V_{oc}, the exact origin of these non-radiative recombination pathways should be investigated in future works.

Methods

References
1. Thompson, B. C. & Fréchet, J. M. J. Polymer-fullerene composite solar cells. *Angew. Chem. Int. Ed.* **47,** 58–77 (2008).
2. Park, S. H. *et al.* Bulk heterojunction solar cells with internal quantum efficiency approaching 100%. *Nature Photon.* **3,** 297–302 (2009).
3. Dennler, G., Scharber, M. C. & Brabec, C. J. Polymer-fullerene bulk-heterojunction solar cells. *Adv. Mater.* **13,** 1323–1338 (2009).

4. Scharber, M. C. *et al.* Design rules for donors in bulk-heterojunction solar cells—towards 10% energy-conversion efficiency. *Adv. Mater.* **18**, 789–794 (2006).
5. Veldman, D., Meskers, S. C. J. & Janssen, R. A. J. The energy of charge-transfer states in electron donor–acceptor blends: Insight into the energy losses in organic solar cells. *Adv. Funct. Mater.* **19**, 1939–1948 (2009).
6. Shockley, W. & Queisser, H. Detailed balance limit of efficiency of p–n junction solar cells. *J. Appl. Phys.* **32**, 510–519 (1961).
7. Gadisa, A., Svensson, M., Andersson, M. R. & Inganäs, O. Correlation between oxidation potential and open-circuit voltage of composite solar cells based on blends of polythiophenes/fullerene derivative. *Appl. Phys. Lett.* **84**, 1609–1611 (2004).
8. Nelson, J., Kirkpatrick, J. & Ravirajan, P. Factors limiting the efficiency of molecular photovoltaic devices. *Phys. Rev. B* **69**, 035337 (2004).
9. Rand, B. P., Burk, D. P. & Forrest, S. R. Offset energies at organic semiconductor heterojunctions and their influence on the open-circuit voltage of thin-film solar cells. *Phys. Rev. B* **75**, 115327 (2007).
10. Potscavage, W. J., Yoo, S. & Kippelen, B. Origin of the open-circuit voltage in multilayer heterojunction organic solar cells. *Appl. Phys. Lett.* **93**, 193308 (2008).
11. Kirchartz, T., Mattheis, J. & Rau, U. Detailed balance theory of excitonic and bulk heterojunction solar cells. *Phys. Rev. B* **78**, 235320 (2008).
12. Benson-Smith, J. J. *et al.* Formation of a ground-state charge-transfer complex in polyfluorene/[6,6]-phenyl-C-61 butyric acid methyl ester (PCBM) blend films and its role in the function of polymer/PCBM solar cells. *Adv. Funct. Mater.* **17**, 451–457 (2007).
13. Loi, M. A. *et al.* Charge transfer excitons in bulk heterojunctions of a polyfluorene copolymer and a fullerene derivative. *Adv. Funct. Mater.* **17**, 2111–2116 (2007).
14. Hallermann, M., Haneder, S. & Da Como, E. Charge-transfer states in conjugated polymer/fullerene blends: Below-gap weakly bound excitons for polymer photovoltaics. *Appl. Phys. Lett.* **93**, 053307 (2008).
15. Veldman, D. *et al.* Compositional and electric field dependence of the dissociation of charge transfer excitons in alternating polyfluorene copolymer/fullerene blends. *J. Am. Chem. Soc.* **130**, 7721–7735 (2008).
16. Kim, H. *et al.* Electroluminescence in polymer-fullerene photovoltaic cells. *Appl. Phys. Lett.* **86**, 183502 (2005).
17. Tvingstedt, K. *et al.* Electroluminescence from charge transfer states in polymer solar cells. *J. Am. Chem. Soc.* **131**, 11819–11824 (2009).
18. Goris, L. *et al.* Absorption phenomena in organic thin films for solar cell applications investigated by photothermal deflection spectroscopy. *J. Mater. Sci.* **40**, 1413–1418 (2005).
19. Goris, L. *et al.* Observation of the subgap optical absorption in polymer-fullerene blend solar cells. *Appl. Phys. Lett.* **88**, 052113 (2006).
20. Vandewal, K. *et al.* The relation between open-circuit voltage and the onset of photocurrent generation by charge-transfer absorption in polymer: fullerene bulk heterojunction solar cells. *Adv. Funct. Mater.* **18**, 2064–2070 (2008).
21. Campoy-Quiles, M. *et al.* Morphology evolution via self-organization and lateral and vertical diffusion in polymer: fullerene solar cell blends. *Nature Mater.* **7**, 158–164 (2008).
22. Ma, W. L., Yang, C. Y., Gong, X., Lee, K. & Heeger, A. J. Thermally stable, efficient polymer solar cells with nanoscale control of the interpenetrating network morphology. *Adv. Funct. Mater.* **15**, 1617–1622 (2005).
23. Peet, J. *et al.* Efficiency enhancement in low-bandgap polymer solar cells by processing with alkane dithiols. *Nature Mater.* **6**, 497–500 (2007).
24. Wienk, M. M. *et al.* Efficient methano[70]fullerene/MDMO-PPV bulk heterojunction photovoltaic cells. *Angew. Chem. Int. Ed.* **42**, 3371–3375 (2003).
25. Vanecek, M. & Poruba, A. Fourier-transform photocurrent spectroscopy of microcrystalline silicon for solar cells. *Appl. Phys. Lett.* **80**, 719–721 (2002).
26. Würfel, P. The chemical potential of radiation. *J. Phys. C* **15**, 3967–3985 (1982).
27. Schick, K., Daub, E., Finkbeiner, S. & Würfel, P. Verification of a generalized Planck law for luminescence radiation from silicon solar cells. *Appl. Phys. A* **54**, 109–114 (1992).
28. Trupke, T., Würfel, P., Uhlendorf, I. & Lauermann, I. Electroluminescence of the dye-sensitized solar cell. *J. Phys. Chem. B* **103**, 1905–1910 (1999).
29. Band, Y. B. & Heller, D. F. Relationships between absorption and emission of light in multilevel systems. *Phys. Rev. A* **38**, 1885–1895 (1988).
30. Ross, R. T. & Calvin, M. Thermodynamics of light emission and free-energy storage in photosynthesis. *Biophys. J.* **7**, 595–614 (1967).
31. Green, M. A. *Third Generation Photovoltaics: Advanced Solar Energy Conversion* (Springer, 2006).
32. Rau, U. Reciprocity relation between photovoltaic quantum efficiency and electroluminescent emission of solar cells. *Phys. Rev. B* **76**, 085303 (2007).
33. Kirchartz, T. & Rau, U. Detailed balance and reciprocity in solar cells. *Phys. Status Solidi A* **205**, 2737–2751 (2008).
34. Bruan, D. Electron injection and conduction processes for polymer devices. *J. Polym. Sci. Part B: Polym. Phys.* **41**, 2622–2629 (2003).
35. Waldauf, C., Scharber, M. C., Schilinsky, P., Hauch, J. A. & Brabec, C. J. Physics of organic bulk heterojunction devices for photovoltaic applications. *J. Appl. Phys.* **99**, 104503 (2006).
36. Panda, P. *et al.* Charge transfer absorption for pi-conjugated polymers and oligomers mixed with electron acceptors. *J. Phys. Chem. B* **111**, 5076–5081 (2007).
37. Foster, R. *Organic Charge-Transfer Complexes* (Academic, 1969).
38. Pope, M. & Swenberg, C. E. *Electronic Processes in Organic Crystals and Polymers* (Oxford Univ. Press, 1999).
39. Ross, R. B. *et al.* Endohedral fullerenes for organic photovoltaic devices. *Nature Mater.* **8**, 208–212 (2009).
40. Lenes, M. *et al.* Fullerene bisadducts for enhanced open-circuit voltages and efficiencies in polymer solar cells. *Adv. Mater* **20**, 2116–2119 (2008).
41. Zhang, F. *et al.* High photovoltage achieved in low band gap polymer solar cells by adjusting energy levels of a polymer with the LUMOs of fullerene derivatives. *J. Mater. Chem.* **18**, 5468–5474 (2008).
42. Perez, M. D., Borek, C., Forrest, S. R. & Thompson, M. E. Molecular and morphological influences on the open circuit voltages of organic photovoltaic devices. *J. Am. Chem. Soc.* **131**, 9281 (2009).

Acknowledgements

Author contributions

K.V. and A.G. prepared the devices and carried out FTPS measurements in Hasselt. K.T. and K.V. prepared devices and carried out the electroluminescence measurements in Linköping. K.V. wrote the paper. All authors provided comments on the manuscript. J.V.M. and O.I. directed the research.

Additional information